Spray Characteristics of a Liquid-Liquid Coaxial Swirl Atomizer at Different Mass Flux Ratios

K. Ghorbanian[1], M.R. Soltani[2]
Sharif University of Technology, Tehran, Iran

and

M. Ashjaee[3]
University of Tehran, Tehran, Iran

and

M.R. Morad[4]
Sharif University of Technology, Tehran, Iran

Abstract

An experimental investigation is performed to explore the characteristics of sprays produced by a liquid-liquid coaxial swirl injector in a non-combusting environment. Phase Doppler anemometry is used for the measurement of velocity and Sauter mean diameter of droplets across and along the injection axis for various inner- and outer mass flow rates. Results of the combined spray are compared with those of inner- and/or outer spray alone. The results indicate that the inner injector has a larger influence on the flowfield of the combined spray compared to the outer one. Further, the maximum velocity of the combined spray is close to the center of the spray thickness and decreases as the distance from the nozzle exit is increased. However, the maximum Sauter mean diameter of droplets along the injection axis moves to the outer periphery and increases as the distance from the nozzle exit is increased.

[1] Assistant Professor
[2] Associate Professor
[3] Associate Professor
[4] Ph.D. Student

Furthermore, the combined spray flowfields are fluid dynamically similar in terms of the velocity and the average Sauter mean diameter of the droplets.

Nomenclature

A_i	Area based on d_i
A_{in}	Area based on d_{in}
A_o	Area based on d_o
$C_{D,i}$	Inner orifice discharge coefficient
$C_{D,o}$	Outer orifice discharge coefficient
d_i	Inner diameter of inner injector orifice
d_{in}	Outer diameter of inner injector orifice
d_{si}	Inner Injector diameter at inlet section
d_{so}	Outer Injector diameter at inlet section
d_o	Inner diameter of outer injector

	orifice
L_{ch}	Characteristic Length
$\dot{m}$	Mass flow rate
r	Radial position
Re	Reynolds number
V	Total velocity
V_{ch}	Characteristic Velocity
$V_{i,\max}$	Inner injector maximum velocity
$V_{o,\max}$	Outer injector maximum velocity
We	Weber number
z	Axial position
ρ_a	Air density
ΔP_l	Liquid pressure drop
ρ_l	Liquid density
σ	Liquid surface tension
μ_l	Liquid Viscosity

Introduction

Liquid fuel/oxidizer atomization is used extensively in rocket engines to exploit their high mixing efficiency within a given length of combustion chamber. As known, atomization processes are inherently complex involving the close coupling of both the thermodynamic state of the fluid as well as the injector design. The state of fragmentation of the injected liquid into smaller fluid elements and its mixing, evaporation, and combination at the molecular level with other species in chemical reaction is of critical importance. Therefore, the characteristics of the resulting spray field have a significant impact on the combustion stability as well as the propulsion efficiency.

Over the past few decades, a series of theoretical and experimental studies are launched in industry and academia towards a better fundamental understanding of the liquid atomization phenomena. Studies are carried out to predict the spray characteristics of coaxial swirl atomizers, emphasizing the velocity as well as the drop size distribution and its influence on the evaporation and mixing of fuel and oxidizer spray. A theoretical study of the liquid film flow on the inner wall of the center post of a swirl injector was performed[1]. The measured spray characteristics exhibited behaviors similar to those of a conventional airblast atomizer. Burick[2] investigated cold flow characteristics of gas/liquid coaxial injectors. Hot wax freezing method was used to study a central liquid sheet surrounded by an annulus gas. It has been found that both the mass flux- and the momentum flux ratios may affect the drop size, mixing, and vaporization efficiencies. Further, photography, patternation, and phase Doppler particle analyzer was employed by Hautman[3] to examine the spray structure of gas/liquid coaxial injectors where the center liquid was swirled. It was observed that the spray structure was similar to those of a pressure swirl injector where the smaller droplets were being entrained into the central region of the spray. In addition, it was reported that the spray angle and the droplet size change as the gas and liquid mass flow rate change. Furthermore, Eroglu

et al[4] and Hardalupas et al[5] employed phase Doppler anemometer (PDA) to look into the local spray characteristics of single coaxial injectors. In the latter report, spray characteristics were examined on the basis of the exit Weber number and the gas-to-liquid velocity ratio. It was reported that for sprays with the same gas-to-liquid velocity ratio, a decrease of liquid tube diameter by 50% improved the atomization by approximately 25% and an increase of the gas-to-liquid velocity ratio enhanced the atomization process. In a different attempt by Hardalupas et al[6], spray characteristics of three identical coaxial air-blast atomizers, placed in a triangular arrangement, were investigated. It was found that downstream merging of the individual sprays was strong in the region between the nozzle axes. Ramamurthi et al[7] investigated the disintegration characteristics of swirled annular liquid sheets of coaxial injectors at different injection pressures. Swirl was generated by a helical swirler and, in some cases, nitrogen gas was injected coaxially over the outer surface of the liquid sheet. The results indicate that coaxial swirl injectors should be designed with large annular clearances and high-centrifugal forces to ensure the formation of annular sheets in the regime of the diverging conical shape.

In another study, Li and Shen[8] used PDA to investigate the spray parameters such as SMD and mean velocity at various radial and axial locations for different gas-to-liquid velocities at the nozzle exit. It was found that the droplet axial velocity had a jet-like self-similar spatial distribution along the radial and axial directions. Sivakumar et al[9] studied the interaction between two conical sheets of liquid, formed by coaxial swirl injectors. Photographic techniques were used to explore the swirling motion, generated by passing the liquids through single start rectangular helical passages. The results indicated that after merging of the two conical liquid sheets, the point of merging moves upstream. In a different attempt, Sivakumar et al[10] investigated the spray characteristics of liquid-liquid coaxial injectors. It was reported that the merging process of liquid sheets leaded to an increase of SMD by 40-50%.

As mentioned above, a series of investigations are conducted on pressure-swirl injectors due to the variety of their application. These studies have explored the effects of nozzle design, operating conditions, properties of liquid and ambient conditions on the spray characteristics such as mean drop size, spray angle, discharge coefficient, and film thickness theoretically and experimentally. However, only limited experimental studies are reported in literature on the detailed spray structures and atomization characteristics resulting from liquid-liquid coaxial swirl (LLCS) atomizers. In LLCS configuration, the liquid fuel and oxidizer are injected into the combustion chamber through the inner and outer orifice of the coaxial swirl injector, respectively. The present work is motivated by a better understanding on the interaction processes between the liquid sheets of liquid-liquid coaxial swirl atomization. An in-house-designed LLCS injector is investigated in terms of velocity as well as drop size distribution at different stations from the injection plane by means of PDA. Further, similitude features are investigated for the spray flowfield.

Experimental Setup and Instrumentation

The present authors have conducted a series of experimental studies on various governing parameters of liquid spray pattern of swirl type injectors[11,12,13,14]. The spray formation of various swirl injectors at different injection pressures as well as different geometrical arrangements are investigated. Spray cone angles, breakup lengths, and velocity components are obtained as a function of pressure drop. At low injection pressures, a high-speed, high-resolution CCD camera is used to visualize the essential features of the liquid sheets and breakup processes whereas at higher pressures, PDA is used for the simultaneous measurement of velocities and droplet sizes in regions of interest. In the present paper, attention is focused on PDA results for an in-house-designed LLCS injector. Liquid is injected simultaneously at different mass flow rates and pressures through the inner as well as

the outer orifice of the coaxial swirl injector, representing fuel and oxidizer flow rates, respectively. A schematic illustration of the injector and its geometric configurations are shown in Fig.1 and Table 1.

Table 1 Geometric configurations

d_i	2.0 *mm*
d_o	5.8 *mm*
$d_o - d_{in}$	2.15 *mm*
d_{si}	6.0 *mm*
d_{so}	9.0 *mm*

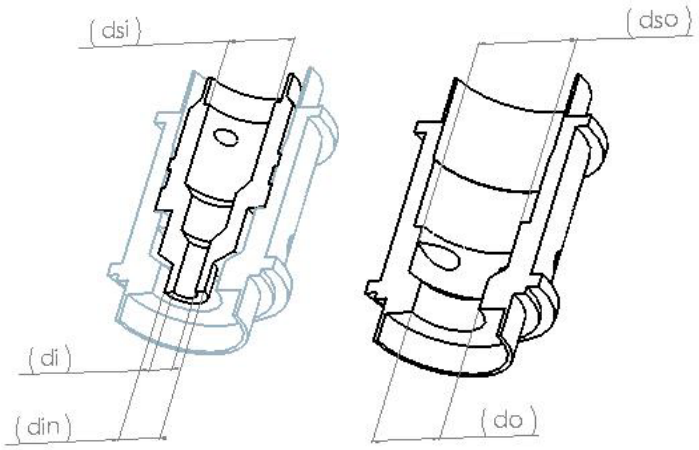

Fig. 1 Schematic of the LLCS injector

It should be mentioned that the swirling motion is generated by passing the liquids through tangential inlet ports with circular cross section. the inner injector has two tangential inlet ports with diameter of $d_{pi} = 1.2\,mm$ and the outer injector has four tangential inlet ports with diameter of $d_{po} = 1.5\,mm$. The swirl intensity, given by the swirl number, S, used by Sivakumar[10], is derived for present coaxial injector for both inner and outer orifices (S_i, S_o respectively).

$$S_i = \frac{d_{si} d_i}{n_i d_{pi}^2}$$

$$S_o = \frac{(d_o - d_{in}) d_{so}}{n_o d_{po}^2}$$

Where n_i, n_o are number of tangential inlets for inner and outer parts, respectively. According to the geometrical dimensions for present coaxial injector, swirl number for the inner injector is $S_i = 4.167$ and for outer injector is $S_o = 2.15$.

Experimental Setup

The experimental setup, as schematically illustrated in Fig.2, consists of two liquid supply systems, an injector mounting system, an optical table for laser diagnostics, and a data acquisition system.

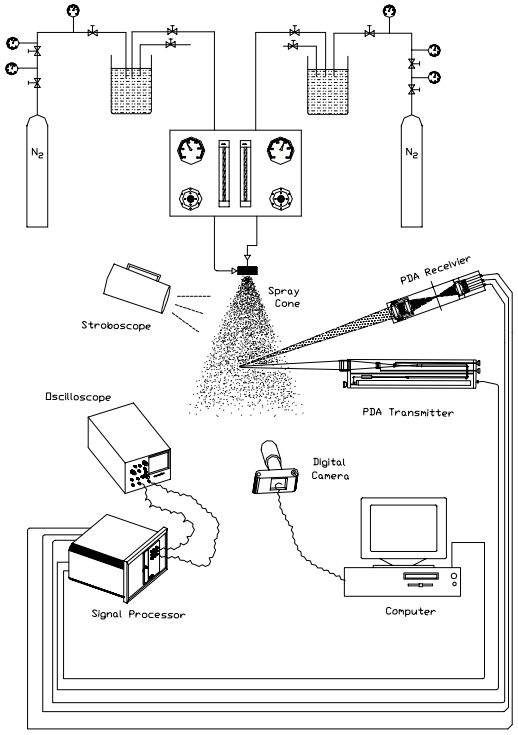

Fig. 2 Schematic of the experimental setup

For the present study, water is used as the test fluid and is supplied to the inner- as well as the outer coaxial swirl injector from different pressurized tanks. The water supply system includes two water tanks, pressurized nitrogen bottles, pressure regulators, flowmeters, and water filters. Further, both water supply systems have a rated maximum pressure of approximately 6.2 MPa (900 psia). The liquid-liquid coaxial swirl injector is mounted on a three-axis traverse system for precise positioning in the horizontal as well as vertical planes with the injector orifice being pointed downwards. In addition, the water spray is injected into a large collection vessel to the ambient condition. The collection vessel is located adequately downstream of the injector ensuring not to interfere with the flowfield being investigated.

Diagnostics

Phase Doppler anemometry is used for the simultaneous measurement of velocities and droplet sizes. PDA is a point measurement technique based upon an extension of the basic principles of the conventional dual-beam laser Doppler velocimeter except that three photo-detectors are used to resolve the ambiguity in the phase angle of the measured optical signals for the determination of droplet sizes.

A coherent multilane argon-ion continuous wave laser is used as the light source. The laser beam is sent to the transmitter where the colors are separated in green (514.5 nm), blue (488 nm), and violet (476.5 nm) for axial and diameter measurements, velocity determination, and laser light extinction measurements, respectively. The laser beam is split into two beams of equal intensity by the transmitting optics, and focused to an intersection to form a probe volume at a point in the spray. The probe volume characteristics are defined by the optical arrangement of the transmitter. A portion of the probe volume is imaged at the slit within the receiver. When a drop crosses the fringe pattern of light in the probe volume, scattered light is received simultaneously by three photo-multiplier tube detectors. The Doppler signal analyzer electronics, and associated software, process the signals from the detectors to simultaneously get droplet size and velocity component perpendicular to the plane of the fringes. A second component of velocity may be obtained by employing an additional pair of laser beams at a different wavelength in a plane orthogonal to the first pair of beams. The additional beam pair forms another probe volume collocated with the first one so that the second velocity component is obtained for the same particle. Finally, the signals are downloaded into a PC for data storage. Detailed information about the optical characteristics of the PDA system is provided by Morad[15].

The PDA transmitting and receiving optics is mounted on a horizontal plane and the PDA laser beams intersect with the spray to form a fringe pattern in the horizontal plane. The

measurements for the droplet size and velocities are based on 3000 samples per point for a maximum duration time of 25 seconds resulting in uncertainties of less than $6\,\mu m$ and $0.5\,m/s$ for SMD of droplets and droplet velocities in the main thickness of the spray cone, respectively. Finally, for flow visualization, spray images are captured by a 640x480 pixel digital camera where a stroboscope is used as the light source.

Transient Spray Formation

As a starting point, the spray formation when discharging through the inner nozzle of the LLCS injector is studied. In a pressure-swirl atomizer, angular momentum is imposed on the liquid to form a swirling motion. Under the action of the centrifugal force, initially, a swirling liquid film emerges axially from the injector exit and forms a swirling hollow cone sheet owing to the azimuthally component of velocity. Small-scale structure is developed on the liquid surface at the exit; however, larger-scale structure quickly dominates the film along the adjacent expanding sheet and the sheet starts to split becoming a series of distorted ligament-like elements. Further, additional breakup may occur due to collision or aerodynamic forces deforming the liquid particles to the point of secondary atomization.

The experimental range of Reynolds numbers, Re, and Weber numbers, We, for both the inner and the outer nozzle sprays are calculated where Re and We are defined as:

$$\mathrm{Re} = \frac{\rho_l V_{ch} L_{ch}}{\mu_l} \qquad \text{and} \qquad \mathrm{We} = \frac{\rho_a V_{ch}^{\,2} L_{ch}}{\sigma} \tag{1}$$

While the characteristic length L_{ch} for the inner spray is set equal to the inner diameter of the inner orifice, for the outer spray, it is defined as the difference of the inner diameter of the outer orifice to the outer diameter of the inner orifice, $d_o - d_{in}$, as illustrated in figure 1. In

addition, the characteristic velocity V_{ch} is set equal to the axial velocities at the corresponding nozzle exits. Finally, a comparison between the experimental range and the engine operational condition is made and good similarity is obtained.

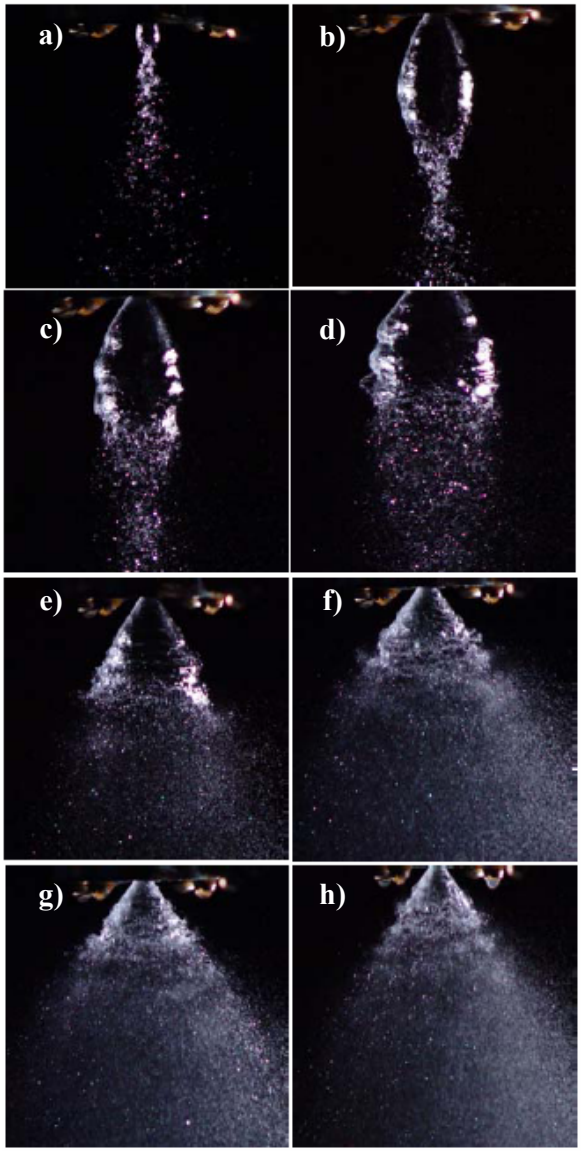

Fig. 3 Spray formation for the inner nozzle of the LLCS injector

Figure 3 shows the development of the spray passing through several stages such as dribble, onion, tulip stages and fully developed spray as the liquid injection pressure for the inner

nozzle is increased from zero. It can be seen by inspection that for very low injection pressures, $(\Delta P < 0.2\,\text{bar})$, a hollow bubble shape of liquid sheet, onion stage, is formed at the nozzle orifice followed by continuous liquid sheet disintegration into drops, Fig. 3a-b. Further, the length of the hollow bubble, which may be considered as the breakup length for this mode, increases with injection pressure. A further increase of the injection pressure will result in sheet instability and thus a semi-burst of the hollow bubble is followed by a transformation into a conical smooth liquid film, tulip stage, Fig. 3c-e. Furthermore, as the distance from the nozzle orifice increases, perforations are developed resulting in a decrease of the sheet thickness. At higher discharging pressure, Fig. 3f, annular waves appear and the liquid sheet experiences wave disturbances – a state in which external forces dominate the surface tension forces in the liquid. Ultimately, wave frequency increases with injection pressure resulting in development of short-length waves as well as shorter breakup lengths. A fully developed spray corresponding to a flow Reynolds number of 62941 is shown in Fig. 3h.

The impact of the spray formation for increasing the discharging pressure for the outer nozzle of the LLCS injector while maintaining the discharging through the inner nozzle at a fixed value is investigated. Figure 4 shows the conditions where the inner nozzle is maintained at an onion stage with a Reynolds number equal to 5000 while the mass flow rate for the outer nozzle is increased from its tulip stage to wavy disintegration mode. It is apparent from Fig. 4 that an increase of the discharging pressure for the outer nozzle will first not affect the onion stage of the inner nozzle; however, at a Reynolds number equal to 25244, it will disintegrate the onion stage of the inner nozzle abruptly to form a combined fully developed spray. Finally, it should be mentioned that a further increase of the discharging pressure for the inner nozzle will shift the Reynolds number for a fully combined spray pattern to lower values for the outer nozzle.

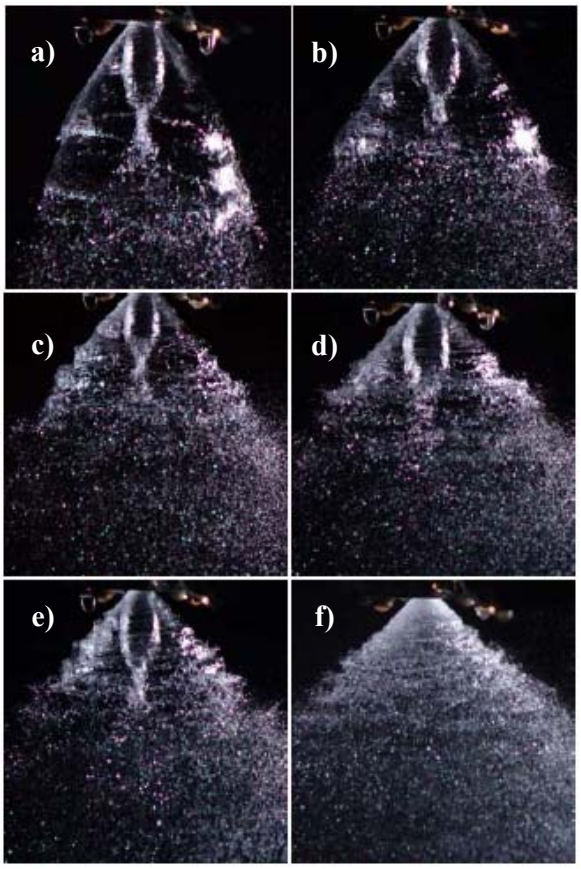

Fig. 4 Spray formation of the LLCS injector of variable and constant discharging pressures for outer- and inner nozzle, respectively.

Fully Developed Test Condition

A sectional view of the spray flowfield is schematically illustrated in figure 5. The coordinate z has its origin located at the nozzle exit and is pointed to the downstream direction of the spray. The coordinate r is normal to the z-coordinate and is in the radial direction of the spray.

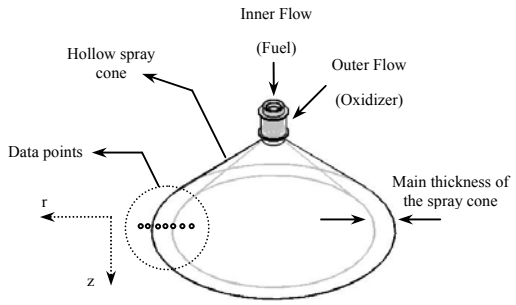

Fig. 5 Schematic of the spray flowfield

In the present paper, measurements are performed along the r-coordinate as well as z-coordinate. Further, the probe volume and the total number of measurement points are selected to ensure measurements across the main thickness of the merged spray sheets but also inside the spray cone of the inner flow (fuel) as well as outside the spray cone of the outer flow (oxidizer) at any test condition presented in this paper. Equally spaced measurement points by 5 mm are selected to capture data starting from the inside region of the air-core to the outside region of the combined spray sheet. Information about the operating conditions is summarized in Table 2.

Table 2 Operating conditions of LLCS injector

Operating Parameters	**Present Study**
Mass flow ratio (MFR)	1.92 - 5.71
Velocity ratio (VR)	0.45 – 1.45
Inner orifice:	
Length-to-diameter ratio	2.15
Liquid density, kg/m^3	998
Mass flow rate, lit/hr	70 – 130
Weber number	9-33
Reynolds number	4×10^4 - 7×10^4

Outer orifice:	
Length-to-diameter ratio	1.1
Liquid density, kg / m^3	998
Mass flow rate, lit / hr	250 – 400
Weber number	3.5-9
Reynolds number	2.5×10^4 - 4×10^4

Experimental Results and Discussion

Two groups of measurements are presented in this paper. First, a parametric study on the mutual influence of the inner and outer spray patterns on each other is performed. In other words, at a fixed z-position but variable r-positions, velocity and SMD distributions are obtained for various inner- and outer Reynolds numbers. Second, the Reynolds numbers of the outer and inner sprays are kept fixed and the velocity and SMD profiles of the combined spray are determined at various z-positions. The range of the Reynolds number for the test condition is similar to the actual injector conditions of interest. PDA validation rates are on the order of 70-90% where higher rate corresponds to the spray main thickness region and lower rates for the hollow regions.

Fully Developed Condition of Individual Coaxial Injectors

As a starting point, measurements are conducted to confirm the precise alignment and centering of the integrated coaxial nozzles as well as the spray symmetry along the z-coordinate. The details of the validation procedure and the measurements are given by Morad[15]. Further, preliminary experiments are performed to identify the initiation point of the fully developed condition of the single injectors independent of each other. It should be mentioned that previous experimental investigation has revealed that the smallest mass flow rate for a stable, constant discharge coefficient coalesces with the initiation of a fully

developed spray pattern[16]. Hence, the effect of the flow rates on the variation of the discharge coefficient of single coaxial injectors is investigated where the discharge coefficient is defined as

$$C_D = \frac{\dot{m}}{A\sqrt{2\rho_L \Delta P_L}} \tag{2}$$

It should be noted that the area, A , in the above equation for the inner and outer sprays is set equal to A_i and $A_o - A_{in}$, respectively. The results for discharging either through the inner nozzle only or the outer nozzle only are shown in figure 6. It can be seen by inspection that the discharge coefficient for the inner nozzle only has a sharp drop and reaches an asymptote at $C_{D,i} = 0.21$ for a mass flow rate of $70\,\mathrm{ltr/hr}$ which is in good agreement with reported data for simplex injectors[17]. However, the discharge coefficient for the outer nozzle only shows a fairly smooth drop and reaches an asymptote at $C_{D,o} = 0.17$ for a mass flow rate of $170\,ltr/hr$.

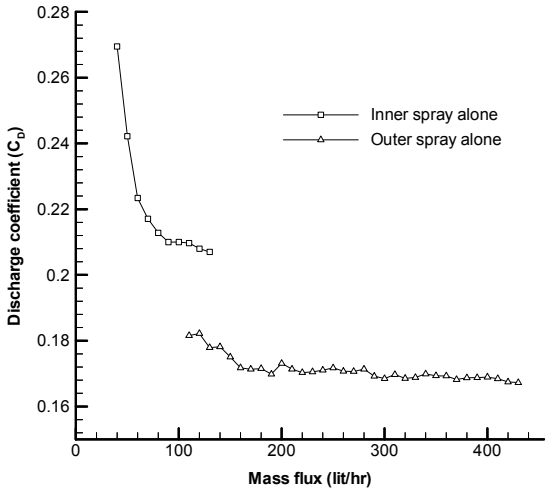

Fig. 6 Variation of the discharge

coefficient with mass flux for inner- and

outer orifices

It is apparent from figure 6, that the values for the lower mass flow rates of the inner- and outer injectors, corresponding to $70 \div 130\, ltr/hr$ and $250 \div 400\, ltr/hr$ as indicated in Table 2, respectively, are within the range of constant discharge coefficients. Further, it is evident that the selected experimental range for the mass flow rates is independent of Reynolds number. In addition, one may calculate the hydraulic discharge area, the axial velocity, and so the Reynolds- and Weber numbers by knowing the discharge coefficient. Hence, for the mass flow rates $70\ ltr/hr$ and $250\ ltr/hr$, the Reynolds numbers are equal to 40047 and 25244. Finally, experiments are also performed to assure that under the fully developed condition the inner spray is always in the air-core of the outer spray.

Normalization

In general, in order to enhance comparison, experimental data for injectors are made dimensionless by values at the outer diameter of the nozzle orifice. However, in the present study for liquid-liquid coaxial injectors, due to the existence of two outer diameters – namely, one for the inner nozzle and one for the outer nozzle – the z- and r-coordinates are made dimensionless with respect to the difference between the outer diameters of the inner- and outer nozzles as follows:

$$\hat{z} = \frac{z}{d_o - d_i} \quad \text{and} \quad \hat{r} = \frac{r}{d_o - d_i} \tag{3}$$

Further, the velocity distribution is also made dimensionless as

$$\hat{V} = \frac{V(r,z)}{V_{ref}} \tag{4}$$

where V_{ref} is the average velocity of the maximum velocities of each injector at the nozzle exit (z=0). In other words:

$$V_{ref} = \frac{V_{i,\max} + V_{o,\max}}{2} \tag{5}$$

where $V_{i,max}$ and $V_{o,max}$ correspond to $[Re_o; Re_i] = [0; 74376]$ and $[Re_o; Re_i] = [40390; 0]$, and are equal to 56.1 and 41.3 m/s, respectively. These maximum velocities used for normalization are obtained based on Bernoulli's equation for a pressure drop to ambient condition. Actual velocities at the nozzle exit have been estimated by using discharge coefficients for inner and outer orifices and the estimated actual velocities are obtained less than maximum velocities used for normalization.

Spray Interaction Processes

Velocity Plane

The velocity profiles at a fixed z-position $(\hat{z} = 10.5)$, variable r-positions $0 \le \hat{r} \le 16$, and different Reynolds numbers are shown in figures 7a-e.

Figure 7a shows the velocity profiles for the outer spray at different Reynolds numbers while there is no flow through the inner injector, $Re_i = 0$. It can be seen by inspection that as one moves along the $\hat{r}$-axis, the velocity $\hat{V}$ first increases from the inside periphery and reaches a maximum somewhere within the spray thickness and then decreases towards the outside periphery of the spray cone. Further, an increase of Re_o will result in a shift of the velocity profile towards higher maximum velocities $\hat{V}_{max}$.

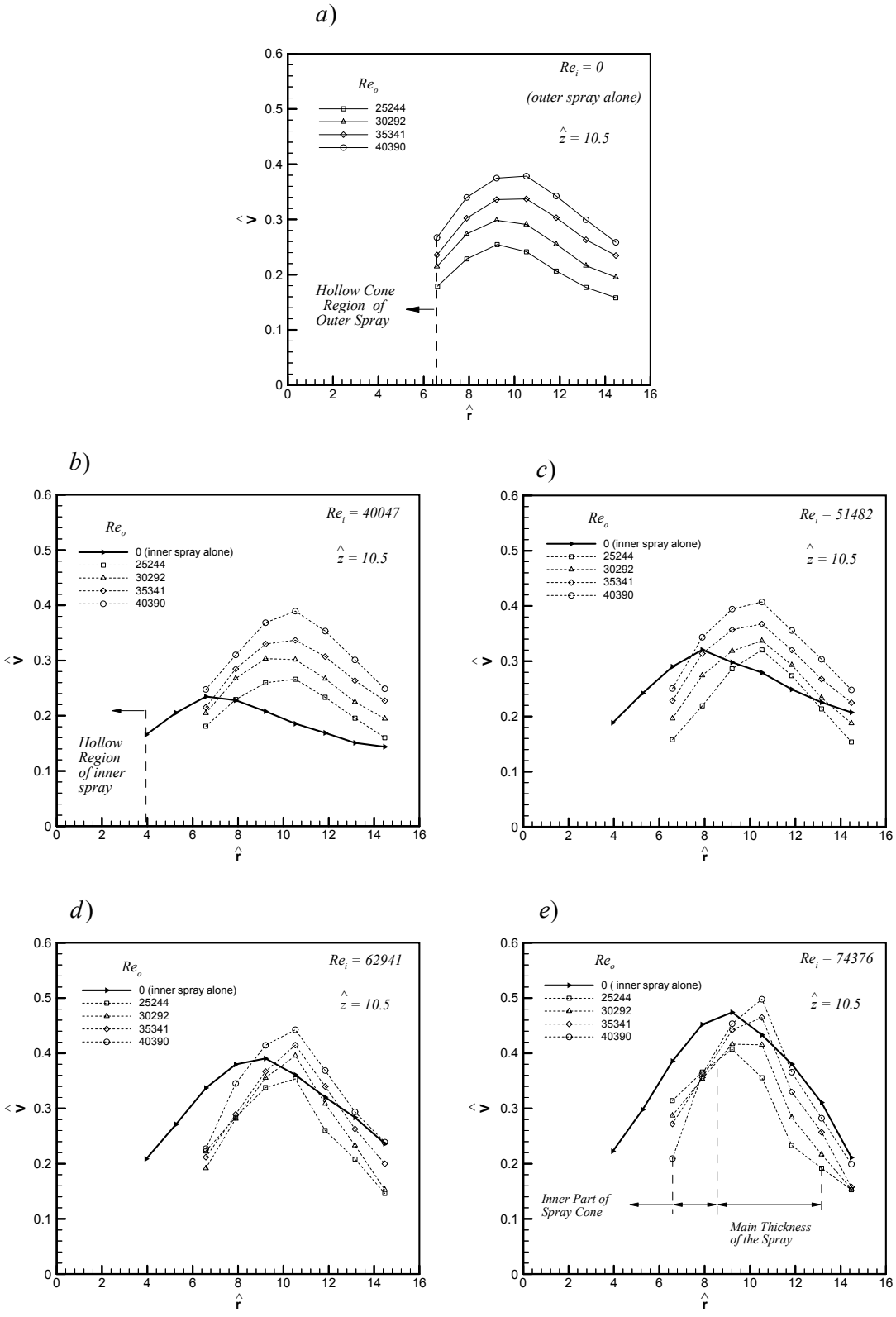

Fig. 7 Velocity distribution for variable $\mathrm{Re_i}$

As a next step, the inner injector is supplied with a flow of initial Reynolds number $\mathrm{Re}_i = 40047$ which is slightly less than the chosen maximum Reynolds number for the outer injector $\mathrm{Re}_o = 40390$. In addition, for interpretation purposes, the velocity profile for which the outer injector is not supplied (that is, the inner spray only) is drawn as a solid line. A comparison between figures 7a and 7b reveals that the combined velocity profiles in figure 7b remain unchanged compared to those in figure 7a. As a result, one may conclude that, under these conditions, the inner Reynolds number $\mathrm{Re}_\mathrm{i} = 40047$ is not strong enough to alter the combined spray pattern in figure 7b. Thus, measurements are carried on for conditions in which the inner Reynolds numbers Re_i are increased up to $\mathrm{Re}_\mathrm{i} = 74376$ (figure 7c-e).

As shown in figure 7c, while the combined velocity profile of $[\mathrm{Re}_\mathrm{i};\mathrm{Re}_\mathrm{o}] = [51482;40390]$ remains almost unchanged, the combined velocity profile corresponding to $[\mathrm{Re}_\mathrm{i};\mathrm{Re}_\mathrm{o}] = [51482;25244]$ is altered and reaches a relatively higher maximum velocity $\hat{\mathrm{V}}_{\max}$. A further increase of the inner Reynolds number $\mathrm{Re}_\mathrm{i} = 62941$, figure 7d, will result in an increase of the maximum velocity $\hat{\mathrm{V}}_{\max}$ of the combined velocity profiles. However, it is important to note that although the combined velocity profile of $[\mathrm{Re}_\mathrm{i};\mathrm{Re}_\mathrm{o}] = [62941;25244]$ is changed compared to those in figures 7a-c; nevertheless, the velocity profile of the inner spray alone, $[\mathrm{Re}_\mathrm{i};\mathrm{Re}_\mathrm{o}] = [62941;0]$, is so significant that its values are larger than those corresponding to $[\mathrm{Re}_\mathrm{i};\mathrm{Re}_\mathrm{o}] = [62941;25244]$ at any point in the spray thickness. This tendency gets stronger as the inner Reynolds number becomes more dominant to the system. As shown in figure 7e, the velocity profile of the inner spray alone, $[\mathrm{Re}_\mathrm{i};\mathrm{Re}_\mathrm{o}] = [74376;0]$, is almost larger than any point of the combined spray patterns. Furthermore, for the combined

velocity profile, while the inner spray cone angle is increased, the outer spray cone angle is slightly decreased compared to the velocity profile corresponding to the inner spray alone $[\mathrm{Re}_o = 0]$, figures 7c-d.

SMD Plane

The SMD of droplets at a fixed z-position $(\hat{z} = 10.5)$, variable $\hat{r}$-positions of $0 \le \hat{r} \le 16$, and different Reynolds numbers corresponding to figures 7a-e are shown in figures 8a-e. Figure 8a shows the SMD profiles for the outer spray at different Reynolds numbers while there is no flow through the inner injector, $\mathrm{Re}_i = 0$. It can be seen by inspection that as one moves along the $\hat{r}$-axis, SMD first increases from the inside periphery and then flattens across the spray thickness. Further, an increase of Re_o will result in a minimal drop of SMD values. However, one may conclude that the SMD profiles for the outer spray alone for various Re_o remain unaffected. Comparison between figures 8b-e reveals that the SMD for droplets of combined sprays, except for those at the inner periphery, are very close to each other and their values are sustained relatively constant for variable inner Reynolds number Re_i. On the other hand, it is apparent that the SMD profiles for the inner spray alone are shifted to lower values for higher Re_i (solid lines in figures 8b-e). Consequently, one may conclude that, under current conditions, the SMD of droplets for the combined sprays remain relatively unaffected by variable Re_i as well as Re_o.

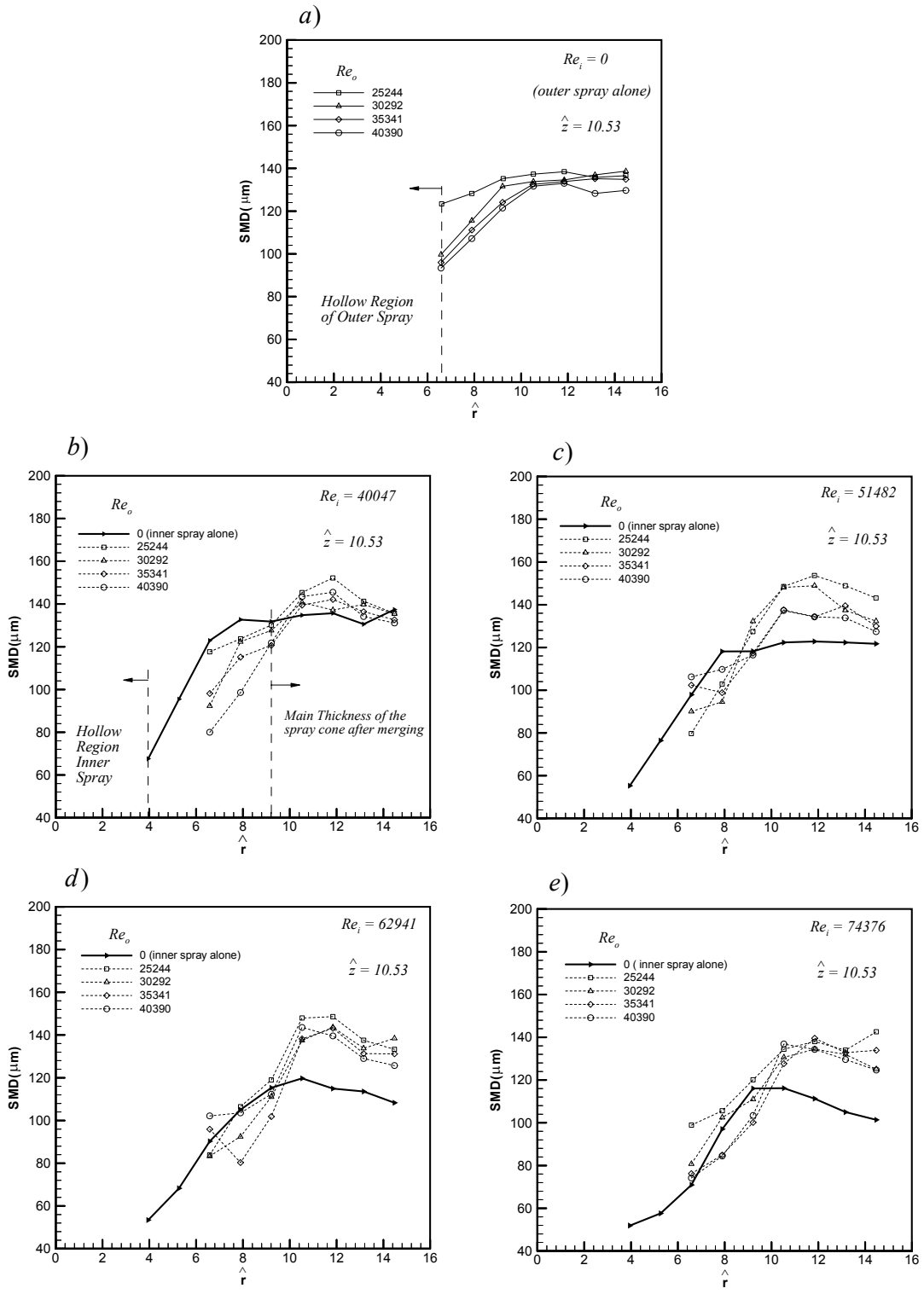

Fig. 8 SMD distribution

Cross-sectional Performance Map

PDA Measurements of the combined sprays at a fixed z-position $(\hat{z}=10.5)$ are summarized in figure 9a-b. While figure 9a illustrates the maximum velocity $\hat{V}_{max}$ of the combined sprays as a function of Re_i and Re_o, figure 9b shows the corresponding averaged SMD of droplets. Hence, one may view figure 9a-b as a cross-section of the performance map of the liquid-liquid coaxial swirl injector. It can be seen that both properties, $\hat{V}_{max}$ and SMD_{avg}, have opposite behavior. In other words, SMD_{avg} decreases with increasing $\hat{V}_{max}$. The properties SMD_{avg} and $\hat{V}_{max}$ possess their lowest and highest value at a point where the Reynolds numbers Re_i and Re_o are the largest, respectively. However, in the present investigation, it is apparent that Re_i has a stronger impact on the atomization efficiency than Re_o. This occurrence may be due to the smaller orifice of the inner injector and its twin-nozzle geometry that provides a higher momentum to the droplets.

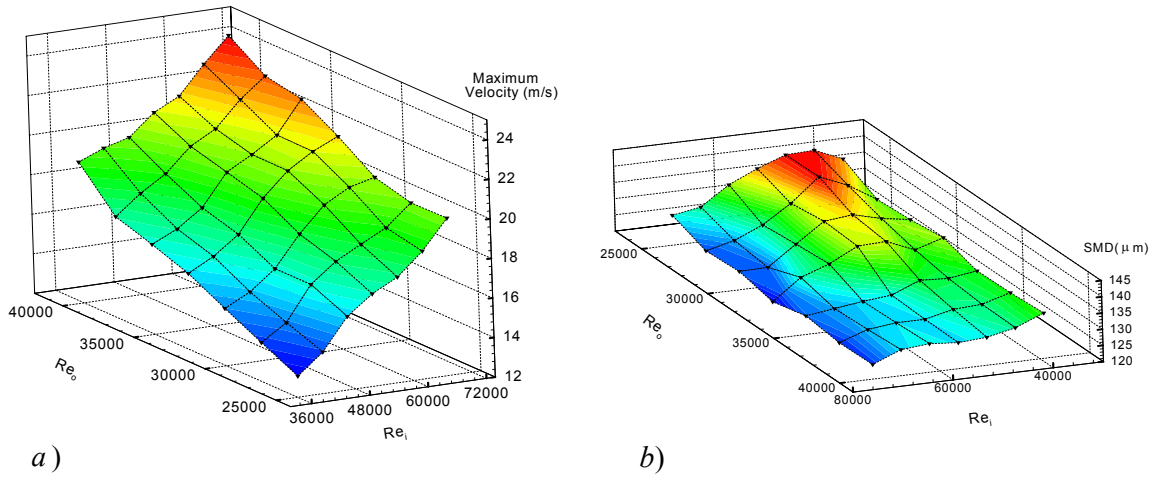

Fig. 9 Performance map for LLCS injector at $(\hat{z}=10.5)$. a)Velocity distribution, b)SMD distribution

Spray Cone Propagation

The downstream variation of velocity distribution and SMD of a combined spray is presented in figures 10 and 11. Measurements are made at various radial positions at six different z-locations and at $[\mathrm{Re}_i;\mathrm{Re}_o]=[57218;30292]$ with $\hat{\mathrm{V}}_{\max}$ and $\mathrm{SMD}_{\mathrm{avg}}$ equal to $17.97\,\mathrm{m/s}$ and $138.8\,\mu\mathrm{m}$, respectively. This condition is similar to the actual operating condition of the injector.

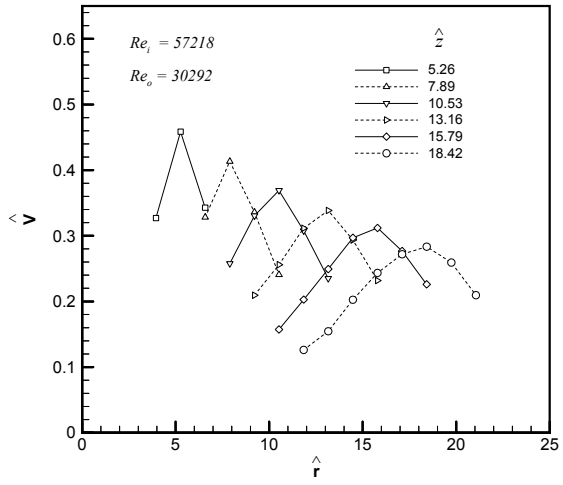

Fig. 10 Downstream variation of the velocity distribution

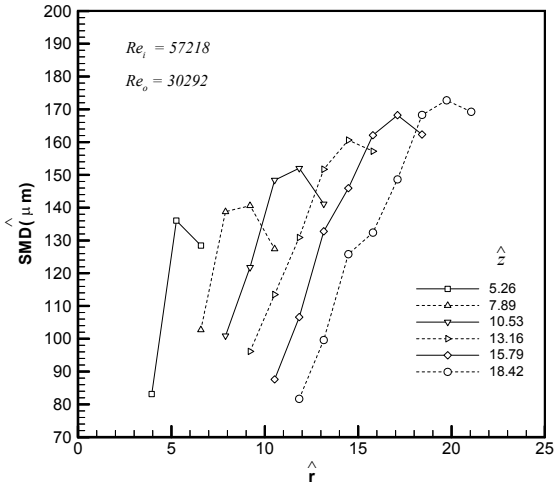

Fig. 11 Downstream variation of SMD distribution

Figure 10 illustrates the spatial distribution of the dimensionless velocity $\hat{V}$. It can be seen by inspection that, at a fixed $\hat{z}$-position, the velocity reaches a maximum value somewhere close to the centerline inside the combined spray thickness and then decreases to the periphery of the spray. Further, along the downstream $\hat{z}$-position, the spray thickness spreads out and the maximum velocity $\hat{V}_{max}$ of the combined spray patterns decreases as the distance from the nozzle exit is increased. From figure 10, it is apparent that the behavior of the droplet velocities $\hat{V}$ at the inner- and outer periphery of the merged spray is different. While, along the downstream z-axis, droplets at the inner periphery are decelerated at a stronger rate than that by $\hat{V}_{max}$, droplets at the outer periphery are almost maintained at the same velocity. However, it is evident that the reduction of the droplet velocities $\hat{V}$ along the inner- and outer peripheries and positions corresponding to $\hat{V}_{max}$ are approximately a linear function.

The corresponding SMD distribution is shown in figure 11. It is apparent that the behavior of the SMD distribution at fixed $\hat{z}$-positions is similar to the corresponding velocity profile. In other words, the SMD of the droplets reaches a maximum value SMD_{max} close to the position of the maximum velocity $\hat{V}_{max}$ and then decreases to the periphery of the spray. However, along the downstream z-axis, the variation of SMD_{max} is opposite to $\hat{V}_{max}$. Near the center, SMD_{max} of the combined spray patterns increases as the distance from the nozzle exit is increased. Further, while SMD increases along the outer periphery to values close to SMD_{max}, it decreases along the inner periphery to smaller values. Finally, a monotonically growth of SMD_{max} with the z-axis is evident.

The foregoing results suggest that along the downstream z-axis the droplets closer to the injector exit have higher velocities than those farther downstream in the spray thickness. Further, as the droplets are transported along the downstream z-axis, velocity profile flattens

due to the loss of its momentum. The results are consistent with Lagrangian analysis on single droplets[18]. Furthermore, the decrease of the SMD along the inner periphery is explained by the occurrence of the additional breakup and vaporization of the droplets on one side and the transportation of relatively small droplets from the central- and outer periphery region of the spray thickness towards the inner periphery on the other side. As a result, larger droplets having larger inertia are migrated from the inner periphery to the central region of the spray describing the monotonically growth of the SMD_{max} .

Self-Similarity

Similitude may be exploited for predicting an injector's drop size and velocity field. The foregoing results offer evidence in favor of the similitude hypotheses assuming that the injector's internal flowfield is one where the inviscid theory applies and injection Reynolds number is in the turbulent range as in the present experiments. Hence, the velocities and SMD of the droplets at each z-position are normalized by the maximum value of the velocity and the maximum value of SMD in the same z-position, respectively:

$$\hat{V}_z = \frac{V(r,z)}{V_{\max}(z)} \quad \text{and} \quad \hat{\mathrm{SMD}}_z = \frac{\mathrm{SMD(r,z)}}{\mathrm{SMD}_{\max}(z)} \tag{6}$$

Further, the normalized coordinate is defined as follows:

$$\hat{r}_z = \frac{r}{z - z_0} \tag{7}$$

where z_0 is considered as the center point of the inner injector and is equal to zero. Figures 12 and 13 show the normalization of the velocity and SMD of the droplets for different r- and z-positions, respectively. It is apparent that while the radial profiles of velocity and SMD are different at various inner- and outer Reynolds numbers, as shown in figures 7 and 8, but the corresponding normalized results corroborates the similitude hypothesis.

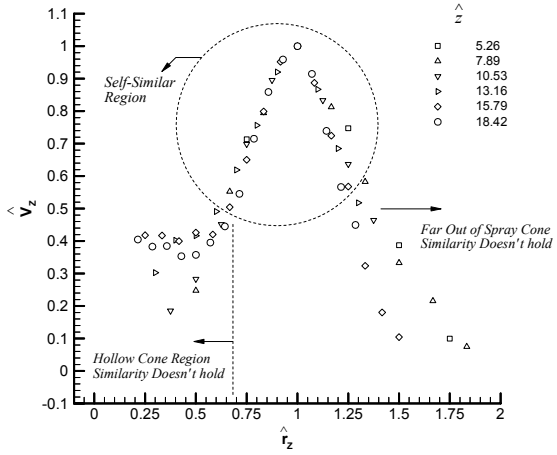

Fig. 12 Normalized velocity distribution

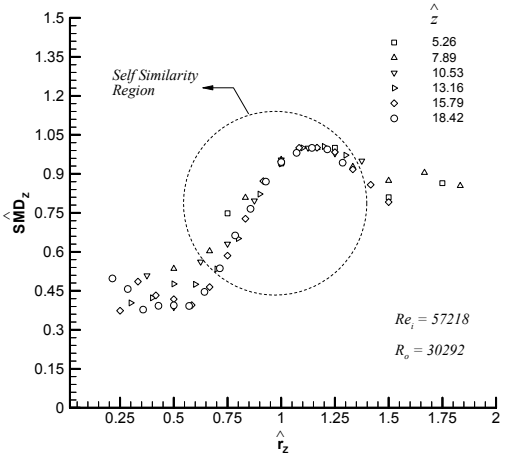

Fig. 13 Normalized SMD distribution

Additionally, figure 12 indicates that the velocity profile is self-similar in the range of $0.67 \le \hat{r}_z \le 1.25$. A closer examination reveals that this range is approximately equal to the spray thickness at the corresponding z-positions. Therefore, points outside the circled region replicate measurements either along the spray periphery or outside the spray. A similar observation is made for $\hat{SMD}_z$ in figure 13. As a result due to self-similar behavior of both

the velocities and SMD of the droplets, one may map the atomization flowfield of a particular liquid-liquid coaxial swirl injector design by simple scaling of available data, hence preventing a large portion of experiments that are needed for optimizing the injector design.

Conclusions

Combustion applications in both rocket and gas turbine propulsion systems require co-injection of fuel and oxidizer in a form that enhances mixing and improves the chemical reaction processes to be completed in a minimum combustor length. Hence, a systematic fluid dynamic study of liquid-liquid coaxial swirl injector in a non-combusting environment is conducted to elucidate the features governing atomization. PDA is used for a comprehensive analysis of velocity and Sauter mean diameter of droplets. Measurements are performed across and along the injection axis for various inner- and outer mass flow rates. Results of the combined spray are compared with those of inner- and/or outer spray alone.

In the present paper, four significant conclusions are obtained from the water spray studies. First, the measurements show that smaller drops are moving slower than the larger ones. Second, it is found that the inner injector has a larger influence on the flowfield of the combined spray compared to the outer injector. Velocity and SMD measurements at a fixed z-position but different inner- and outer mass flow rates indicate that, for the velocity distribution, the variation of the inner Reynolds number Re_i has a stronger impact on the combined spray than any variation of the outer Reynolds number Re_o. Further, the Sauter mean diameter of the droplets for the combined spray at a fixed inner Reynolds number Re_i remain relatively unaffected by variable outer Reynolds number, Re_o.

Third, assessment of the downstream variation of the flowfield of a combined spray for inner- and outer mass flow rates similar to the real operating conditions revealed the opposite

behavior of the maximum velocity to the maximum Sauter mean diameter. It is found that while, $\hat{V}_{max}$ of the combined spray, which is close to the center of the spray thickness, decreases as the distance from the nozzle exit is increased, SMD_{max} moves to the outer periphery and increases as the distance from the nozzle exit is increased.

Finally, normalization of velocity and SMD measurements from different flowfields that are produced by the injector at different flow rates are found to collapse. The results reveal that the combined spray flowfields are in fact fluid dynamically similar both in terms of the velocity as well as the Sauter mean diameter of the droplets that vary with the radial position.

In conclusion, results confirm expectations that although sheet breakup occurs much closer to the injector exit, this does not necessarily result in much smaller drops. It is well known that atomization is a result of the forces of inertia and surface tension acting on the fluid leaving the injector. Therefore, the fineness of the spray depends upon whether the liquid stream momentum is high enough to cause significantly liquid/liquid shear interactions. In addition, it should be noted that there is momentum exchange between the injection liquid sheets and the ambient stagnant gas as well. Hence, the combined spray results from a three-way interaction between liquid/liquid and ambient gas.

Finally, it should be emphasized that second order effects such as the boundary layer thickness within the film, the injector wall roughness, the tube exit lip condition, and so forth, do exist and could have a measurable effect on the resulting flowfield. In the present paper, the second order effects are not investigated and assumed to be negligible. Therefore, further investigation is required to explore these and whether the surface tension or the aerodynamic forces are dominant in the force balance in order to establish the physical mechanisms governing atomization.

Acknowledgement

The financial support of the Sharif University of Technology is gratefully acknowledged.

References

[1] Inamura, T., Tamura, H., and Sakamoto, H., "Characteristics of Liquid Film and Spray Injected from Swirl Coaxial Injector", *Journal of propulsion and Power*, Vol. 19, No. 4, July-August 2003, pp. 632-639.

[2]Burick, R. J., "Atomization and Mixing Characteristics of Gas/Liquid Coaxial Injector Elements," *Journal of Spacecraft and Rockets*, Vol. 9, No. 5, 1972, pp. 326-331

[3]Hautman, D. J., "Spray Characterization of Liquid/Gas Coaxial Injectors with the Center Liquid Swirled," *Atomization and Sprays*, Vol. 3, 1993, pp. 373-387.

[4]Eroglu, H., and Chigier, N. A., "Initial Drop Size and Velocity Distributions for Airblast Coaxial Atomizers," *Journal of Fluid Engineering*, Vol. 113, 1991, pp. 453-459.

[5]Hardalupas, Y., and Whitelaw, J. H., "Characteristics of Sprays Produced by Coaxial Airblast Atomizers," *Journal of Propulsion and Power*, Vol. 10, No. 4, 1994, pp. 453-460.

[6]Hardalupas, Y., and Whitelaw, J. H., "Interaction Between Sprays From Multiple Coaxial Airblast Atomizers," *Journal of Fluid Engineering*, Vol. 118, 1996, pp. 762-771.

[7]Ramamurthi, K., and Tharakan, T. J., "Experimental Study of Liquid Sheets Formed in Coaxial Swirl Injectors" *Journal of Propulsion and Power*, Vol. 11, No. 6, 1995, pp. 1103-1109.

[8]Li, X., and Shen, J., "Experimental Study of Sprays from Annular Liquid Jet Breakup" Journal of Propulsion and Power, Vol. 15, No. 1, 1999, pp. 103-110.

[9]Sivakumar, D., and Raghunandan, B. N., "Jet Interaction in Liquid-Liquid Coaxial Injectors," *Journal of Fluid Engineering*, Vol. 118, 1996, pp. 329-334.

[10]Sivakumar, D., and Raghunandan, B. N., "Role of Geometric Parameters on the Drop Size Characteristics of Liquid-Liquid Coaxial Swirl Atomizers", *Atomization and Sprays*, Vol. 8, 1998, pp. 547-563.

[11]Ghorbanian, K., Ashjaee, M., Soltani, M. R., Mesbahi, M. H., and Morad, M. R., "Experimental Study of the Spray of a Liquid-Liquid Coaxial Swirl Injector for Different Injection Pressures", *9th International Conference on Liquid Atomization and Spray Systems*, ICLASS 2003, Sorrento, Italy, 2003.

[12] Ghorbanian, K., Ashjaee, M., Soltani, M. R., Mesbahi, M. H., and Morad, M. R., "PDA Droplet Size and Velocity Measurement of a Swirl Atomized Spray", *9th Asian Congress of Fluid Mechanics*, Isfahan, Iran, 2002.

[13]Ashjaee, M., Soltani, M.R., Ghorbanian, K., and Morad, M.R., "PDA Study of Two Phase Flow in a Spray Field of a Jet- Swirl Type Injector", *3rd Australian Conference on Laser Diagnostics in Fluid Mechanics and Combustion*, Australia, 2002.

[14]Ashjaee, M., Ghorbanian, K., Soltani, M. R., Mesbahi, M. H., and Morad, M. R., "PDA Measurements of Droplet Size and Velocity In Mixing Region of Two Sprays", *9th Conference of Iranian Society of Mechanical Engineers*, Tehran, Iran, 2002.

[15] Morad, M. R., "Determination of the Spray Characteristics of a Liquid-Liquid Coaxial Injector Utilizing PDA and Neural Network Analysis", Sharif University of Technology, March 2004.

[16] Ghorbanian, K., Ashjaee, M., Soltani, M. R., Mesbahi, M. H., and Morad, M. R., "Experimental Flow Visualization of Single Swirl Spray Pattern at Various Pressure Drops", *AIAA 39th Joint Propulsion Conference and Exhibit*, Huntsville, Alabama, USA, 20-23 July 2003. AIAA-2003-4758.

[17] Suyari, M. and Lefebvre, A. H., "Film Thickness Measurements in a Simplex Swirl Atomizer", *Journal of Propulsion,* Vol. 2, No. 6, 1986, pp 528-533.

[18] Morad, M.R., Soltani, M.R., Ashjaee, M., and Ghorbanian, K., "Experimental Study and a Lagrangian Modeling of Droplet Velocity for the Spray of A Swirl Atomizer", *4th Iranian Aerospace Society Conference*, Amirkabir University of Technology, Tehran, Iran, 2003.